Open access • Journal Article • DOI:10.1126/SCIENCE.1243641

Low Coseismic Friction on the Tohoku-Oki Fault Determined from Temperature Measurements — Source link

Patrick M. Fulton, Emily E. Brodsky, Yasuyuki Kano, Jim Mori ...+8 more authors

Institutions: University of California, Santa Cruz, Kyoto University, Texas A&M University, Japan Agency for Marine-Earth Science and Technology ...+1 more institutions

Published on: 06 Dec 2013 - Science (American Association for the Advancement of Science)

Topics: Elastic-rebound theory, Moment magnitude scale and Slip (materials science)

www.sciencemag.org/cgi/content/full/342/6163/1214/DC1

Supplementary Materials for

Low Coseismic Friction on the Tohoku-Oki Fault Determined from Temperature Measurements

P. M. Fulton,* E. E. Brodsky, Y. Kano, J. Mori, F. Chester, T. Ishikawa, R. N. Harris, W. Lin, N. Eguchi, S. Toczko, Expedition 343, 343T, and KR13-08 Scientists

*Corresponding author. E-mail: pfulton@ucsc.edu

Published 6 December 2013, *Science* **342**, 1214 (2013)
DOI: 10.1126/science.1243641

This PDF file includes:

Materials and Methods

Temperature Data

Temperature data were collected with 55 miniature temperature loggers (MTLs): 10 TDR-2050s and 15 TR-1050s manufactured by RBR Ltd. (Canada; **www.rbr-global.com/**) and 30 Antares 1357 high-pressure data loggers manufactured by Antares Datensysteme GmbH (Germany; **www.antares-geo.de/**). Each of the MTLs has an autonomous data logger and a temperature sensor enclosed within a titanium casing pressure rated for up to 10,000 m water depth. The TDR-2050s also have a pressure sensor that effectively records the sensor's water depth inside the cased borehole. The MTLs were attached to spectra rope and wrapped with a rubber protective covering. The sensor string was attached to a hanger and hung within 4.5" steel tube casing with a check-valve at the bottom that prohibited fluids from flowing into the casing from below. Spacing between sensors varied from 1.5 m at the bottom near the fault zone to 3 m, 6 m and greater intervals higher up. The sensors recorded every 10s, 20s or 10 minutes depending upon the model. The RBR temperature sensors have precision of <0.00005°C and the Antares 0.001°C. In addition to factory calibration constants, each temperature sensor was calibrated using a Hart Scientific water bath containing a mixture of ethylene glycol and water and an NIST reference temperature probe over 8 or more different temperatures from 0 – 30^{o}C and spanning the range recorded during the JFAST experiment. The resulting sensor corrections permit accuracy for all temperature sensors to within ~0.001^{o}C. Reliable corrections could not be obtained for sensors at 744.77 and 805.17 mbsf. The absolute temperatures for these two sensors may be off by a few 10^{-3} ^{o}C , although their residual temperatures appear consistent with neighboring data. Additional details regarding the sensors and observatory are described in (*13*).

Thermal Properties

Knowledge of thermal-physical rock properties is important for interpreting the temperature data. Differences in thermal conductivity may lead to steady-state perturbations in the background geothermal gradient. Estimates of the thermal diffusivity are important for interpreting an observed temperature anomaly from frictional heating, and volumetric heat capacity controls the relationship between heat and temperature. We utilize thermal property measurements taken on core material from borehole C0019E that cover lithologic and depth intervals that correspond to the regions covered by sensors in the observatory. Thermal conductivity values consist of 45 shipboard measurements on split cores using a TEKA thermal conductivity half-space probe (*13*). An additional 38 discrete samples were also measured using a divided bar system revealing similar results. Four large samples were also measured using the transient plane heat source method revealing very little anisotropy in thermal conductivity. Thermal diffusivity and heat capacity measurements were also determined for these four samples. The lowermost three samples are most representative of the intervals covered by sensors and the fault zone with the frictional heat signal and reveal average diffusivity and volumetric heat capacity values of $3.92 \pm 0.5 \times 10^{-7}$ m^2s^{-1} and 2.804 ± 0.32 MJ $^{o}C^{-1}m^{-3}$. Large systematic changes in thermal conductivity are not observed over the intervals covered by temperature sensors (Fig. S2). There is, however, some difference in volumetric heat capacity and thermal diffusivity between the lowermost sample within subducting pelagic clays most

representative of the décollement fault zone and overlying mudrocks. This variability accounts for the largest source of uncertainty in our dissipated energy estimates.

Background geotherm / vertical heat flow

The average background geothermal gradient in the area of the frictional heat anomaly is calculated using a least-squares fit to data from 650 – 750 mbsf (n=18). This depth interval covers the hanging wall of the décollement where there is both abundant temperature and thermal conductivity data and above the frictional heat anomaly and areas of suspected heat advection by fluid flow. The data used for the fit are the daily average temperatures from an arbitrary day, 6 Dec 2012, that is well after drilling and installation so as to minimize any residual effects of drilling disturbance and before the nearby 7 Dec 2012 M_w7.4 earthquake which resulted in temperature perturbations. This value is relatively consistent throughout this time period, although there is a gradual steepening of the gradient due to reequilibration of the hole after drilling (Fig. S3). Error ranges reported in the main text for the gradient are 1 standard deviation determined by bootstrapping with 1000 realizations.

Thermal conductivity and temperature measurements are from separate boreholes, and thus we calculate the vertical heat flow by multiplying the least-squares fit thermal gradient by the average thermal conductivity values corresponding to the same depth and lithologic interval. To remove the background gradient for analysis of residual temperature (i.e. temperature minus a constant average background geotherm) we also utilize a least squares fit to the 5 data representative of positions above 650 mbsf (Fig. S1). Together the composite average background geotherm starts from a projected temperature at the sea floor of 2.50°C and increases by 27.57°C km^{-1} until 650 mbsf and then continues by 26.29°C km^{-1} to the bottom of the sensor string. The projected seafloor temperature of 2.50°C is larger than the observations taken at the seafloor of 1.7°C suggesting that thermal conductivity decreases at depths shallower than those covered by the observatory sensors.

Thermal conductivity as source of anomaly

If the thermal conductivity around the bottom part of the sensor string is much lower than the rest of the measurement depth range, it can result in a higher thermal gradient and hence a positive temperature anomaly as observed. Likewise, an increase in thermal conductivity can lead to a lower thermal gradient. The thermal conductivity λ necessary for a ΔT anomaly over a depth interval Δz is

$$\lambda = q_0 \Big/ \left(\frac{q_0}{\lambda_0} + \frac{\Delta T}{\Delta z} \right) \qquad \text{(S1)},$$

where q_o and λ_o are the background vertical heat flow (30.50 ± 2.52 mW m^{-2}) and thermal conductivity (1.16 ± 0.09 W m^{-1} °C^{-1} above the décollement fault zone), respectively.

Based on the JFAST observations, a 0.31°C anomaly spread over ~20 m would require a thermal conductivity of 0.73 W m^{-1} °C^{-1} in the fault zone if the anomaly resulted from thermal conductivity variations alone.

Core samples within and around the décollement fault zone have a bulk thermal conductivity of 1.14 ± 0.07 W m^{-1} $^oC^{-1}$ and porosities of 35.9 – 52.5% implying matrix values of λ_m ~ 1.39 – 2.13 W m^{-1} $^oC^{-1}$. Bulk thermal conductivity λ_b for intimately mixed phases is appropriately modeled by:

$$\sqrt{\lambda_B} = \phi\sqrt{\lambda_w} + (1-\phi)\sqrt{\lambda_m} \qquad \text{(S2)},$$

where ϕ is porosity, λ_m is matrix conductivity, and λ_f is thermal conductivity of water which equals 0.6 W m^{-1} $^oC^{-1}$ (*21*). Considering similar composition and λ_m value, a bulk thermal conductivity of 0.73 W m^{-1} $^oC^{-1}$ requires porosities of 80 – 88%. Such large porosities are not apparent in logging or core observations from adjacent holes, suggesting thermal conductivity variation is an unlikely source for the observed positive heat anomaly along the plate boundary.

A localized increase in porosity by just 10% over a 20 m wide zone could result in reduction in thermal conductivity to values ~ 1.01 – 1.04 W m^{-1} $^oC^{-1}$ and an apparent positive temperature anomaly by 0.05 – 0.07 ^{o}C. Direct measurements of thermal conductivity, including four measurements on highly sheared sections of the fault zone core itself, show no indication of such a large-scale systematic change in thermal conductivity within or around the fault zone (Fig. S2).

Drilling Anomaly

The perturbation due to drilling is modeled with a two-part synthetic. During drilling, seawater is circulated in the hole, and it is appropriately modeled as an isothermal line-source for the duration of drilling following reference (*8*). Heat is diffused axisymmetrically around the borehole. The resultant temperature disturbance as a function of time is

$$\Delta T_1(z,t) = [T_f - T_0(z)]\frac{Ei(-r_b^2/4\alpha(t-t_2)) - Ei(r_b^2/4\alpha(t-t_1(z))}{Ei(-r_b^2/4\alpha(t_2-t_1(z)))} \qquad \text{(S3)},$$

where T_f is the fluid temperature, $T_0(z)$ the rock temperature at the time of drilling, *Ei* is the exponential integral, r_b is the borehole radius, α is the thermal diffusivity of the formation, $t_1(z)$ is the time since the bit first penetrated to depth z, t_2 is the time drilling ends and fluid is no longer circulated.

During the casing installation, a cold pipe is lowered into the hole providing an instantaneous line sink of heat. On the center axis, the temperature disturbance is

$$\Delta T_2(z,t) = [T_c - T_0(z)](1 - e^{r_b^2/4\alpha(t-t_c(z))}) \quad \text{(S4)},$$

where T_c is the casing temperature, and as before, $t_c(z)$ is the time of installation of the casing at depth z (*22*, p. 260).

Diffusion Model

The frictional temperature anomaly is modeled by the diffusion of heat from an infinitesimally thin planar source into the surrounding media. Although the thickness of a finite shear zone (*2a*) is important for constraining the maximum peak temperature within the fault during the earthquake, it is not a significant parameter for calculating the residual temperature anomaly at times longer than the characteristic diffusion time across the shear layer ($a^2/4\alpha$). The maximum possible thickness of the shear layer within the décollement plate boundary fault is 4.86 m (*6*) and commonly faults localize slip on zones on the order of 0.1-1 cm thick (*23*). The data studied here begin more than 1 year after the earthquake, so the appropriate model for the current data set is an infinitesimally thin plane:

$$\Delta T_{EQ}(z,t) = \frac{S}{2\sqrt{\pi\alpha(t-t_{EQ})}} e^{-(z-z_f)^2/4\alpha(t-t_{EQ})} \qquad \text{(S5)},$$

where t_{EQ} is the time of the earthquake, z_f is the depth of the fault, and the heat source, *S,* is the energy per m^2 dissipated by friction, i.e., $S=\tau d$ where τ is the shear stress on the fault during the earthquake and *d* is the slip distance. The recorded temperature as a function of depth and time is modeled as

$$T(z,t) - \left(\frac{dT}{dz}\right)_{gt} z = \Delta T_1 + \Delta T_2 + \Delta T_{EQ} \quad \text{(S6)}.$$

The most direct constraint from the data is on the dissipated energy *S.* Since the displacement is constrained from repeat seafloor bathymetry, the shear resistance τ is also readily interpretable. However, friction on faults is usually parameterized in terms of apparent coefficients of friction. Therefore, we take the extra step of relating the shear stresses to the equivalent apparent coefficient of friction by estimating the effective normal stress at the fault depth assuming hydrostatic pore pressure. The dip of the fault plane is low (5^o) and for a near-horizontal fault zone the effective normal stress is equivalent to the effective overburden stress. For hydrostatic pore pressure, this is defined as,

$$\sigma_n' = \sigma_v' = (\rho_r - \rho_w) gz \qquad \text{(S7)}.$$

Inversion Procedure

We inverted for the best-fit dissipated energy and depth by performing a gridsearch through apparent friction and depth and finding the combination of values that maximized the cross-correlation between the data from 800-820 mbsf and the model from 1 Aug through 6 Dec 2012 (Figs. 3 and S4-S5). For a given friction and depth combination, dissipated energy is uniquely determined and therefore the results can also be viewed as an optimization of dissipated energy and depth. Confidence intervals in Table S2 were computed by varying the thermal diffusivity and heat capacity with a normal distribution over their observed ranges (Table S1) and repeating the inversion for each realization of these thermal parameters (Fig. S6). The depth-constrained inversion

assumed that the fault lies near the observed peak in the temperature between the deepest and the 3rd from the bottom sensor (Fig. 3).

We also calculated confidence intervals based on constant thermal parameters and bootstrapping the observed data. This procedure resulted in much smaller ranges of the inverted parameters. Therefore, the estimates based on a distribution of thermal parameters are preferred as a more accurate representation of the larger source of error.

Radiated Energy

Radiated energy estimates (*11*, *12*) range from 3-9 x 10^{17} J, and assuming 5.4 x 10^{10} m^2 for the rupture area, result in an areal average of 8-17 MJ/m^2.

Peak Temperature During Slip

Although the observed temperature anomaly more than a year after the Tohoku-Oki earthquake is insensitive to the slip zone thickness and slip duration, by assuming these two parameters, estimates of the maximum peak temperature during slip can be made.

The temperature evolution of a frictional heat anomaly T for all times during and after slip can be described by (*24* adapted from *22, 25)*,

$$T(x,t)=\frac{A_\circ}{\rho c}\left(\begin{array}{l} t\left[1-2i^2erfc\left(\frac{a-x}{\sqrt{4\alpha t}}\right)-2i^2erfc\left(\frac{a+x}{\sqrt{4\alpha t}}\right)\right] \\ -H\left(t-t^*\right)\left(t-t^*\right)\left[1-2i^2erfc\left(\frac{a-x}{\sqrt{4\alpha\left(t-t^*\right)}}\right)-2i^2erfc\left(\frac{a+x}{\sqrt{4\alpha\left(t-t^*\right)}}\right)\right] \end{array}\right)$$

(S8a),

for distances $x \leq a$, where a is the half-width of the shear zone, and

$$T(x,t)=\frac{A_\circ}{\rho c}\left(\begin{array}{l} t\left[2i^2erfc\left(\frac{x-a}{\sqrt{4\alpha t}}\right)-2i^2erfc\left(\frac{x+a}{\sqrt{4\alpha t}}\right)\right] \\ -H\left(t-t^*\right)\left(t-t^*\right)\left[2i^2erfc\left(\frac{x-a}{\sqrt{4\alpha\left(t-t^*\right)}}\right)-2i^2erfc\left(\frac{x+a}{\sqrt{4\alpha\left(t-t^*\right)}}\right)\right] \end{array}\right)$$

(S8b),

for $x > a$, where t^* is the duration of heating (i.e. slip duration), α is the thermal diffusivity, ρ and c are the bulk density and heat capacity, respectively. The $i^2erfc(\xi)$ terms represent the second integral of the complementary error function evaluated from ξ to ∞ (*22*), and $H(\xi)$ is the Heaviside function, which is evaluated for $\xi = t - t^*$ such that the multiplied terms to the right are only applied when $t \geq t^*$. A_o is the volumetric frictional heat generation rate within the slip zone defined as

$$A_o = \frac{\tau d}{2at^*} \qquad \text{(S9)},$$

where d is the total slip distance on a particular slip zone. At times considerably greater than the characteristic diffusion time across the slip zone ($t >> a^2/4\alpha$), the results of Eq. S8 and Eq. S5 become indistinguishable.

The maximum peak temperature above the background value occurs at $t = t^*$ and $x = 0$. Using the estimate for the average shear stress during slip τ determined above from the observed temperature anomaly, the maximum peak temperature increase is

$$\Delta T_{peak} = \frac{\tau d}{2a\rho c}\left(1 - 4i^2 erfc\left(\frac{a}{\sqrt{4\alpha t^*}}\right)\right) \qquad \text{(S10)}.$$

This equation assumes a constant slip velocity and shear stress during slip, which is a practical approximation that provides a reasonable estimate of peak temperature rise for comparison with geologic and geochemical indicators of frictional heating. Figure S7 shows results for a range of plausible slip durations and slip zone thicknesses.

Geochemical constraints on hydrogeology

Geochemical analysis of pore waters collected from Hole C0019E core samples provides insight into the hydrogeology of the JFAST site subsurface (Fig. S8). The Cl^- concentrations of pore waters are similar to seawater (SW), and a steady decrease from 800 mbsf to the bottom of the hole is observed. Such a decrease of Cl^- is generally explained by contribution of deep-seated fluid, which has been diluted with fresh water derived from the breakdown of hydrous minerals, such as illitization of subducted clay minerals. However, only a slight decrease of Cl^- is observed here (3% dilution) indicating limited contribution of deep-seated fluid compared to, for example, the décollement at the western Nankai trough (20% dilution; *26*). A striking feature of the depth profiles in C0019E is that most of major and minor components analyzed show steady-state increase/decrease below 800 mbsf. Such steady-state characteristics can be explained by vertical diffusive flow combined with in-situ diagenetic solid-fluid reaction (*26*). These observations combined with a lack of minimum or maximum around 820 mbsf suggests no significant active fluid flow along the plate boundary fault.

Other constraints on hydrogeology

Annular pressure while drilling borehole C0019B showed no indication of large overpressures or substantial fluid flow through any faults or fractures, including the décollement (*13*). The pressure data also show no evidence of large fluid losses into highly permeable faults or formations.

Zones of increased permeability, however, are more likely susceptible to a near-borehole infiltration of cold drilling fluids and thus a longer recovery of temperature from drilling disturbance and transient cold anomalies in early times. A depth profile of the characteristic recovery time of temperatures following drilling and observatory installation reveal two zones with anomalously long recovery times around 757 – 769

mbsf and 795 – 811 mbsf (Fig. S9). Both of these zones also record disturbances following a nearby M_w7.4 20 km deep normal faulting earthquake on 7 Dec 2012. Borehole circulation resulting from strong ground motions perturbs borehole temperature in the deeper parts of the borehole before quickly re-equilibrating with the formation. In addition, a gradual increase in temperature over ~1-2 weeks after the local earthquake is seen around 763 – 775 and 803 – 814 mbsf which may be indicative of transient fluid flow from depth up permeable conduits (Fig. 2, S9).

Variability in temperature as indicator of advection

High-frequency variability in the daily-average temperature is clearly apparent at both 784 mbsf and 763 mbsf during periods when advective fluid flow in inferred within these zones (i.e. before and after the local 7 December 2012 earthquake, respectively) (Fig. S9). This temperature variability is correlative with neighboring sensors as well, suggestive of fluctuations in the degree of advective fluid flow over time. We quantify the variability in temperature fluid flow by using a band-pass filter from 2.1 to 3.5 days and taking the standard deviation (Fig. S9D). We analyze the data at all depths for time periods from 1 August to 5 December 2012 to represent times before the local M_w7.4 7 December 2012 earthquake. After the earthquake we analyze times from 10 December 2012 (after a few days of borehole re-equilibration following strong motion disturbance) to 24 April, 2013. The locations of large variability are consistent with other indications of high permeability. The data within the décollement fault zone at ~820 mbsf do not reveal large variability, providing additional evidence to suggest the anomaly at this depth is not a result of, or largely affected by, advective fluid flow.

Supplementary Text

Additional Author notes:

The list of group author "Expedition 343, 343T, and KR13-08 scientists": Masanori Kyo (CDEX-JAMSTEC, Japan), Yasuhiro Namba (CDEX-JAMSTEC, Japan), Hiroaki Muraki (Marine Works Japan, Japan), Takafumi Kasaya (JAMSTEC, Japan), Marianne Conin (CEREGE, France, now at UAG, LARGE, Guadeloupe, France), J. Casey Moore (University of California Santa Cruz), Yasuyuki Nakamura (JAMSTEC, Japan), Louise Anderson (University of Leicester, UK), Becky Cook (University of Southampton, UK), Tamara Jeppson (University of Wisconsin-Madison, USA), Monica Wolfson-Schwehr (University of New Hampshire, USA), Yoshinori Sanada (JAMSTEC, Japan), Saneatsu Saito (JAMSTEC, Japan), Yukari Kido (JAMSTEC, Japan), Takehiro Hirose (JAMSTEC, Japan), Jan H. Behrmann (GEOMAR, Germany), Matt Ikari (University of Bremen, Germany), Kohtaro Ujiie (University of Tsukuba, Japan), Christie Rowe (McGill University, Canada), James Kirkpatrick (Colorado State University, USA), Santanu Bose (University of Calcutta, India), Christine Regalla (The Pennsylvania State University, USA), Francesca Remitti (Universitá Modena e Reggio Emilia, Italy), Virginia Toy (University of Otago, New Zealand), Toshiaki Mishima (Osaka City University, Japan), Tao Yang (Institute of Geophysics, China Earthquake Administration, China), Tianhaozhe Sun (University of Victoria, Canada), James Sample (Northern Arizona University, USA), Ken Takai (JAMSTEC, Japan), Jun Kameda (Hokkaido University, Japan), Lena Maeda (JAMSTEC, Japan), Shuichi Kodaira (JAMSTEC,

Japan), Ryota Hino (Tohoku University, Japan), Demian Saffer (The Pennsylvania State University, USA).

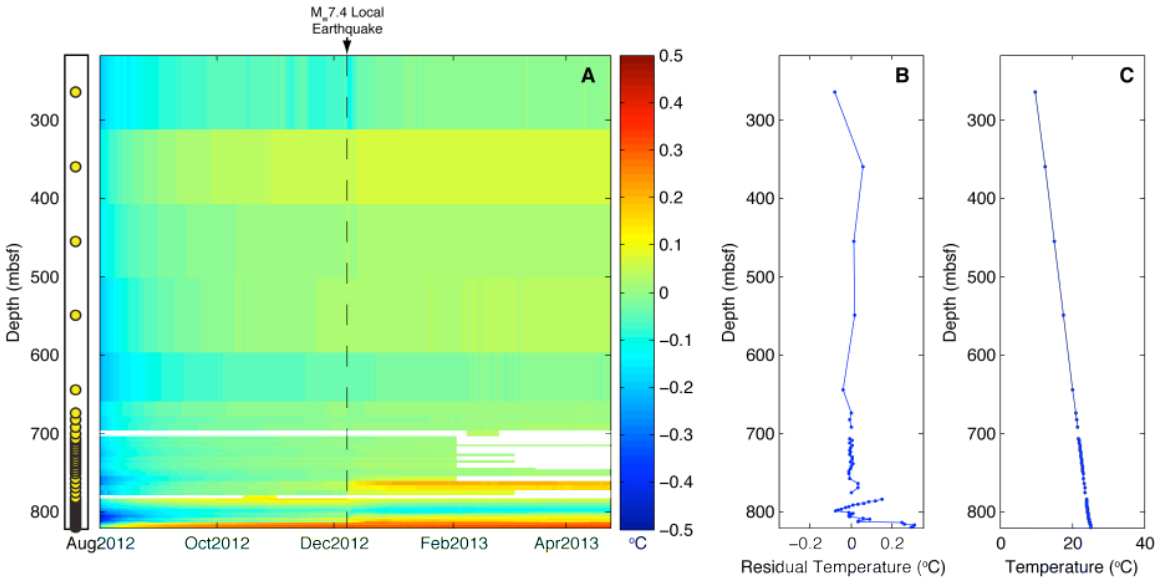

Fig. S1.

Sub–sea-floor residual temperature field. Similar to Fig. 2. (A) Time-space map of all data between 1 August 2012 and 24 April 2013. A close up view of data >650 mbsf is shown in Fig. 2. Yellow dots show sensor positions and each row represents each sensor's data. Each column is the daily average temperature after an average background geotherm is removed. A local M_w7.4 earthquake occurred 17:18:30 JST on 7 Dec 2012 (dashed line). The second deepest sensor (818.51 mbsf) failed on 22 Sept 2012; subsequent data in that row is interpolated from sensors 1.5 m above and below. Periods of no data collection are otherwise shown by white. (B) Depth profile from 1 Dec 2012. (C) Depth profile from 1 Dec 2012 of temperature without background geotherm removed.

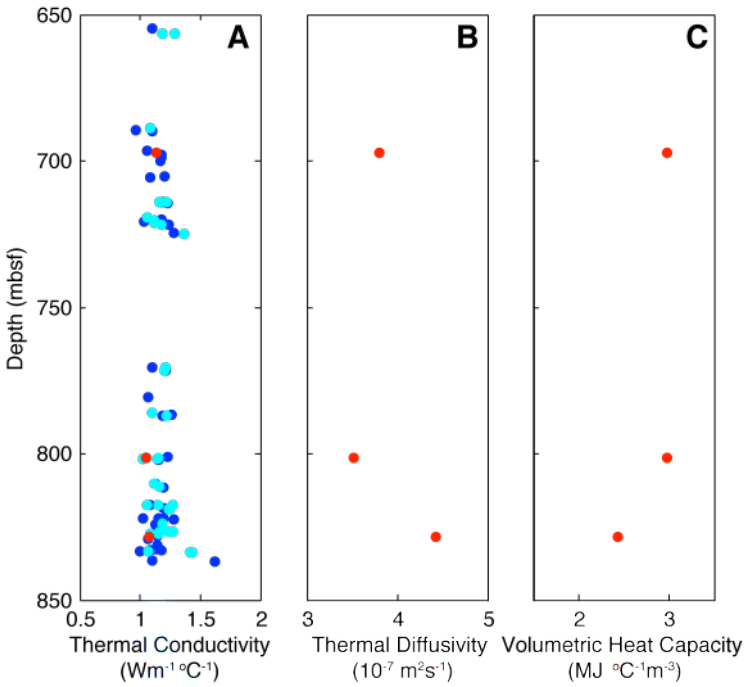

Fig. S2

Thermal Properties. (A) Thermal conductivity, (B) thermal diffusivity, and (C) volumetric heat capacity. All measurements were performed on core samples from hole C0019E. Colors represent data source: blue (*13*); cyan (divided bar measurements); red (transient plane heat source measurements).

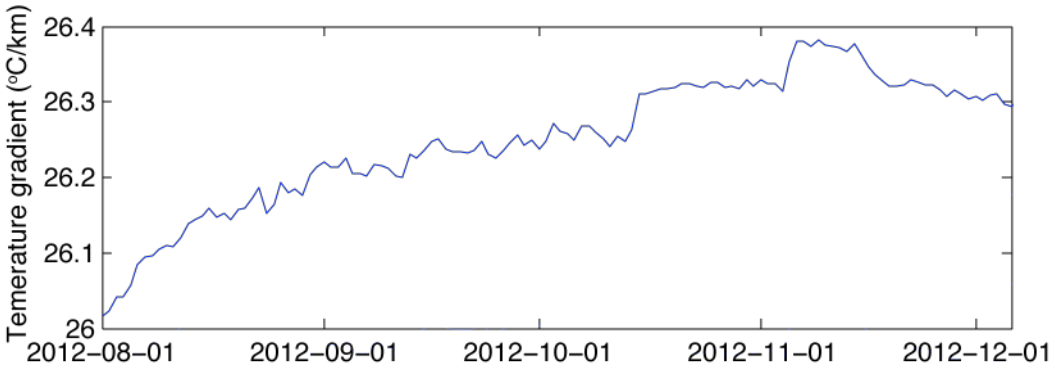

Fig. S3

Temperature gradient over time. Least-squares fit temperature gradient for data between 650 and 750 mbsf for times between 1 August 2012 to 6 Dec 2013.

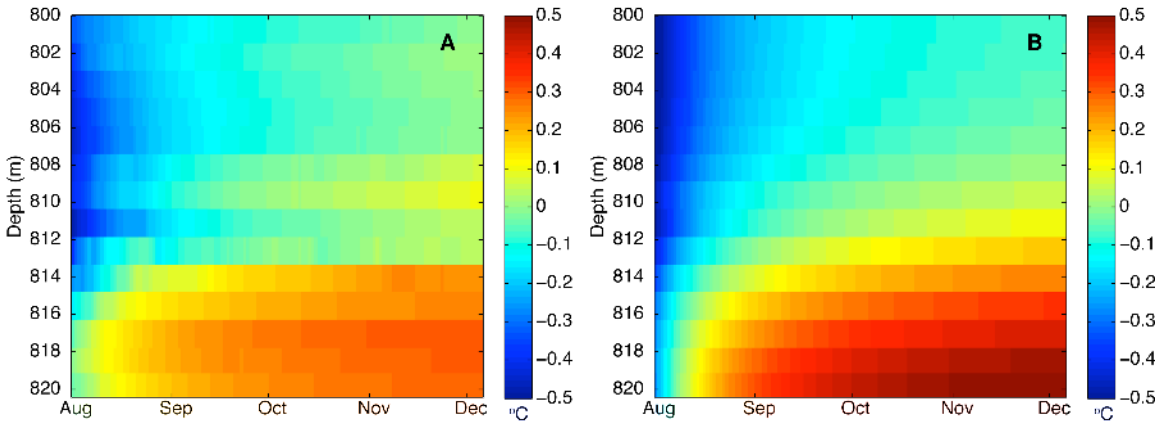

Fig. S4

Time-space map of residual temperature near inferred slip zones. (A) The same as Fig. 3A, a close-up view of the residual temperature anomaly near the plate boundary from 1 August to 6 December 2012. (B) Simulated residual temperature from model inversions in which fault depth is unconstrained.

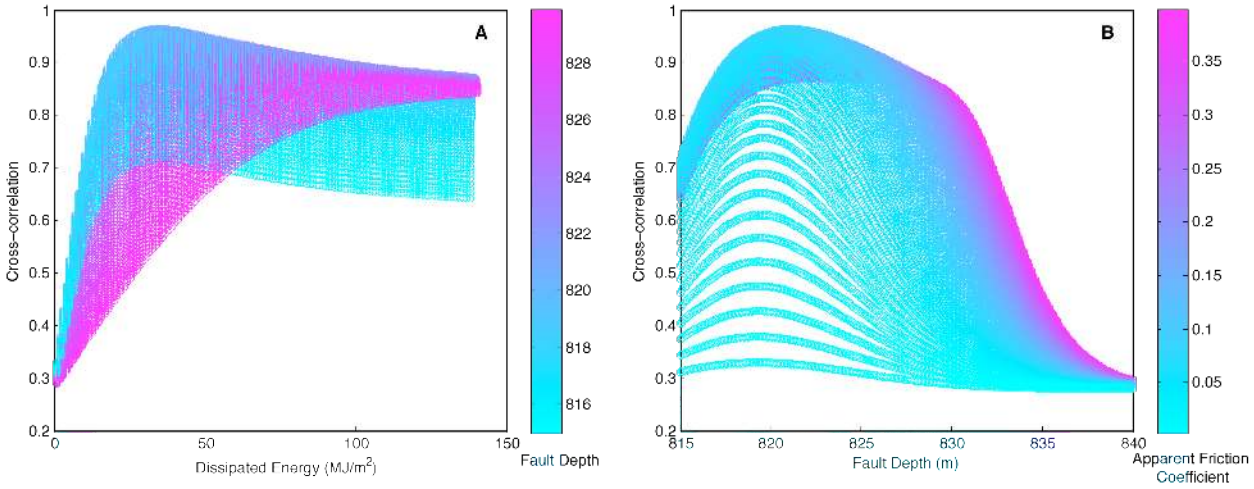

Fig. S5

Cross-correlation of residual temperature from model and observed data for a wide range of depths. Free parameters were apparent coefficient of friction and the depth of the fault. Panel A shows the cross-correlation for different dissipated energy values with color indicating different fault depth locations. Panel B shows the cross-correlation as a function of fault depth with color indicating the apparent friction coefficient derived from different values of dissipated energy.

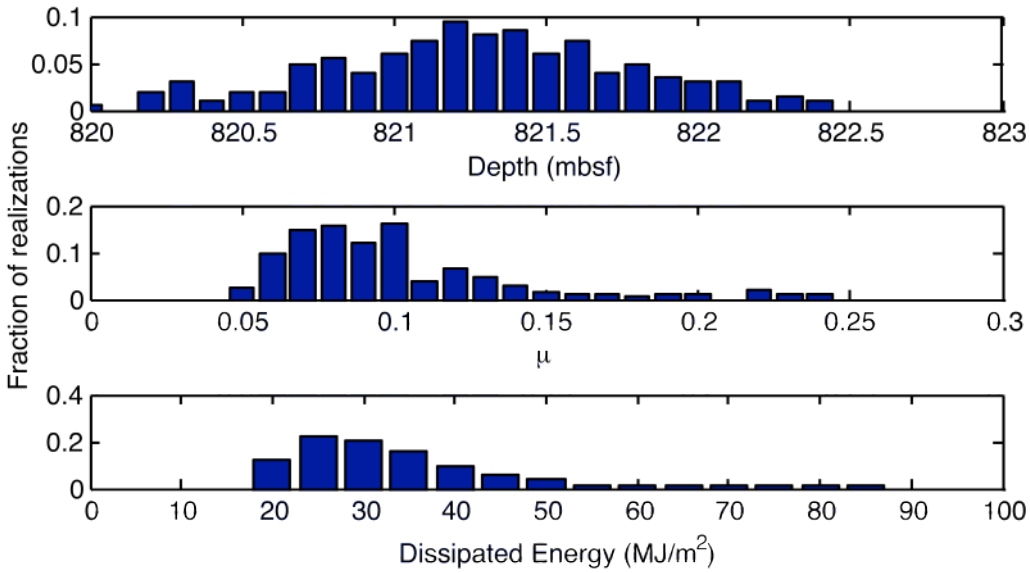

Fig. S6

Normalized distribution of optimal fault depth, apparent friction coefficient μ, and dissipated energy from 200 model inversion realizations with unconstrained depth. The variability in the inversion results stems from allowing the thermal diffusivity and heat capacity to randomly vary over their measured ranges (See text).

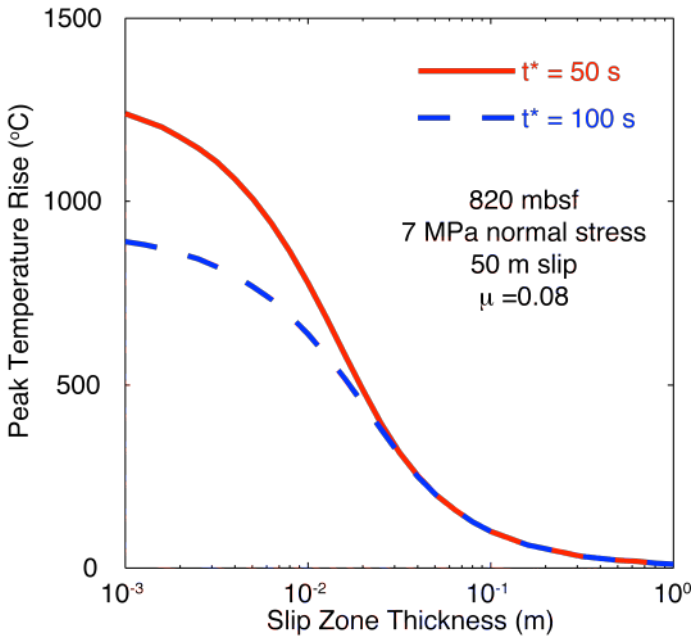

Fig. S7

Peak temperature estimate. Estimate of peak temperature within the fault slip zone for different assumed slip zone thicknesses and slip durations.

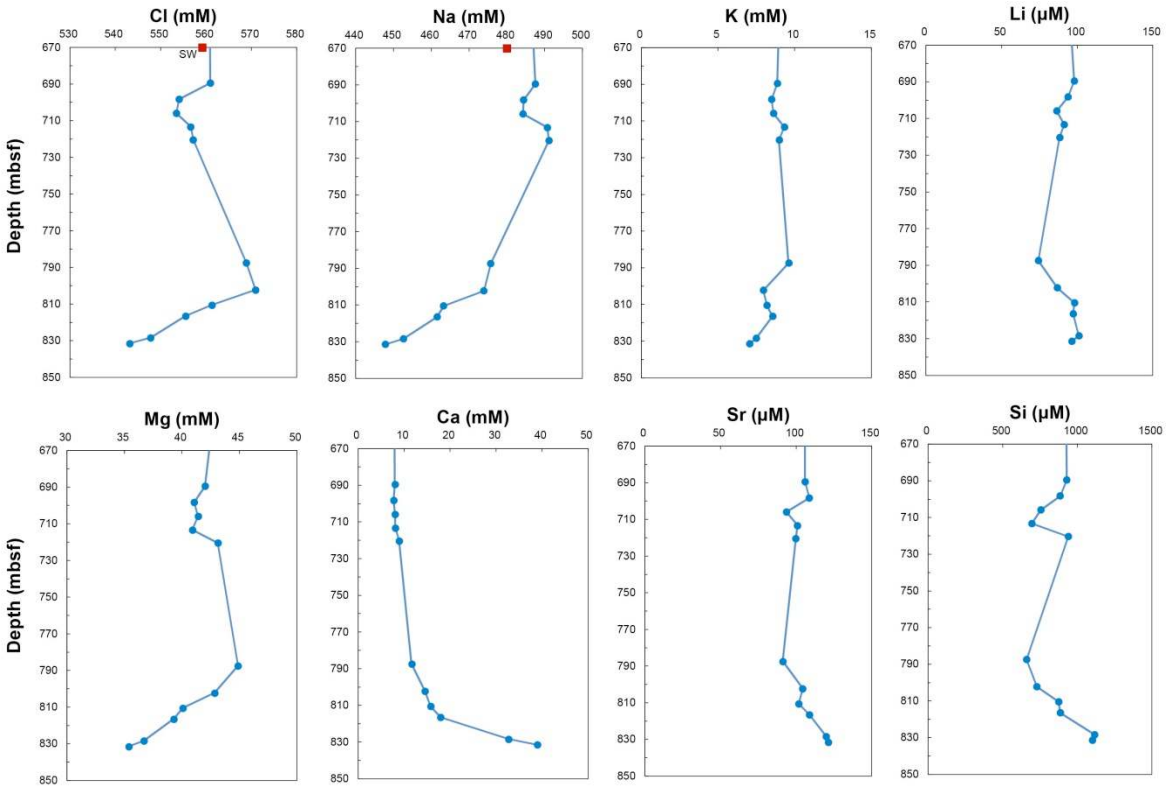

Fig. S8

Pore water geochemistry. Depth profiles of representative pore water geochemistry data from Hole C0019E (*13).*

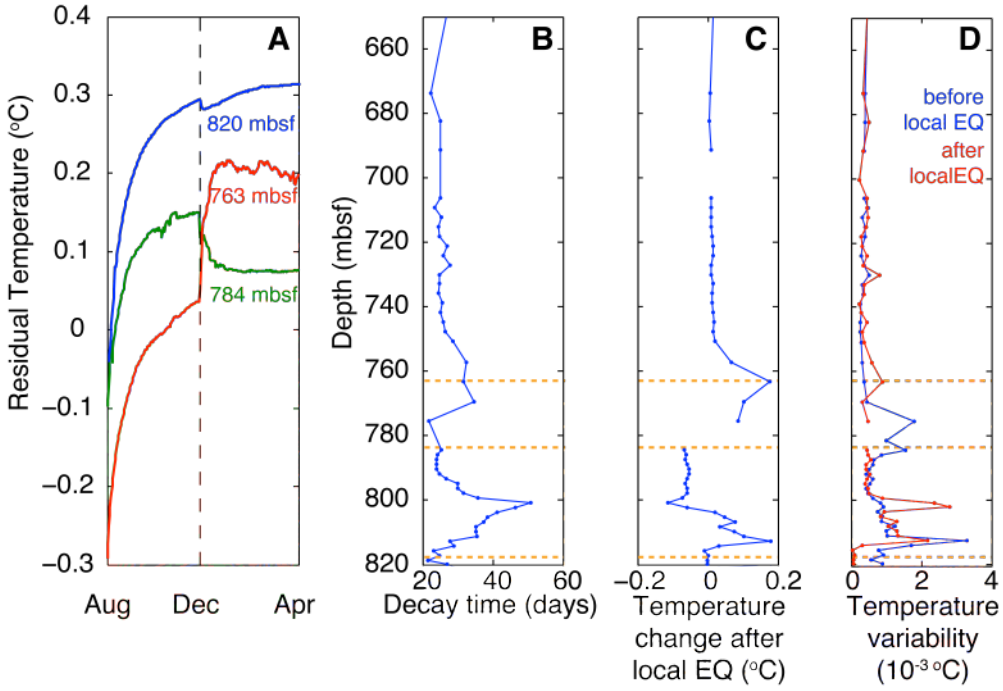

Fig. S9

Permeability Indicators. (A) Time evolution of residual temperature at the plate boundary at around 820 mbsf (blue), 784 mbsf (green), and 763 mbsf (red). Time of M_w7.4 local earthquake on 7 Dec 2012 is shown by dashed line. (B) Depth profile of the characteristic decay time at each sensor depth. Anomalously high decay times may indicate areas of permeable fractures / damage zones in which cold drilling fluids were able to infiltrate during drilling. Locations of 820, 784, and 763 mbsf are shown by orange dashed lines. (C) Change in residual temperature in response to the M_w7.4 local earthquake on 7 Dec 2012 calculated as difference in mean daily temperature at each depth between 6 Jan 2013 and 6 Dec 2013. (D) The standard deviation in temperature variability, as described in the supplemental text, for times before the local 7 Dec 2012 earthquake (blue) and times after the earthquake (red).

Table S1.
Modeling Parameters.

Parameter	Value	
Drilling fluid temperature T_f	1.7°C	Measured seafloor temperature
Casing temperature T_c	1.7°C	Measured seafloor temperature
Thermal diffusivity α	$3.92 \pm 0.05 \times 10^{-7}$ $m^2 s^{-1}$	Average of 3 representative samples
Thermal conductivity K	1.14 ± 0.07 W m^{-1} $°C^{-1}$	Average of 38 representative samples
Volumetric heat capacity ρc	2.804 ± 0.32 MJ $°C^{-1} m^{-3}$	Average of 3 representative samples
Borehole radius r_b	0.1079 m	
Geothermal Gradient $(dT/dz)_{gt}$	26.293°C km^{-1}	Measured
Slip distance d	50 m	*(10)*
Density of rock	1850 kg m^{-3}	Measured on discrete samples >650mbsf (*13*)
Density of water	1000 kg m^{-3}	

Table S2.

Inversion results and confidence intervals.

Depth Constrained inversion	**Median Value**	**90% Confidence Interval**
Depth	819.8 mbsf (7717.3 mbsl)	819.8 mbsf (7717.3 mbsl)
Apparent coefficient of friction	0.08	0.05-0.15
Dissipated energy	27 MJ/m^2	19-51
Slip-averaged shear stress	0.54 MPa	0.38-1.0 MPa
Unconstrained inversion		
Depth	821.3 mbsf (7718.8 mbsl)	820.3-822.1 mbsf (7717.8 -7719.6 mbsl)
Apparent coefficient of friction	0.09	0.06-0.20
Dissipated energy	31 MJ/m^2	20-69 MJ/m^2
Slip-averaged shear stress	0.63 MPa	0.40-1.4 MPa

References and Notes

1. J. Byerlee, Friction of rocks. *Pure Appl. Geophys.* **116**, 615–626 (1978). doi:10.1007/BF00876528

2. G. Di Toro, R. Han, T. Hirose, N. De Paola, S. Nielsen, K. Mizoguchi, F. Ferri, M. Cocco, T. Shimamoto, Fault lubrication during earthquakes. *Nature* **471**, 494–498 (2011). Medline doi:10.1038/nature09838

3. E. E. Brodsky, K.-F. Ma, J. Mori, D. M. Saffer, *Sci. Drill.* 10.2204/iodp.sd.8.11.2009 (2009).

4. Y. Kano, J. Mori, R. Fujio, H. Ito, T. Yanagidani, S. Nakao, K.-F. Ma, Heat signature on the Chelungpu fault associated with the 1999 Chi-Chi, Taiwan earthquake. *Geophys. Res. Lett.* **33**, L14306 (2006). doi:10.1029/2006GL026733

5. H. Tanaka, W. M. Chen, C. Y. Wang, K. F. Ma, N. Urata, J. Mori, M. Ando, Frictional heat from faulting of the 1999 Chi-Chi, Taiwan earthquake. *Geophys. Res. Lett.* **33**, L16316 (2006). doi:10.1029/2006GL026673

6. F. M. Chester, C. Rowe, K. Ujiie, J. Kirkpatrick, C. Regalla, F. Remitti, J. C. Moore, V. Toy, M. Wolfson-Schwehr, S. Bose, J. Kameda, J. J. Mori, E. E. Brodsky, N. Eguchi, S. Toczko, Expedition 343 and 343T Scientists, Structure and composition of the plate-boundary slip zone for the 2011 Tohoku-Oki earthquake. *Science* **342**, 1208 (2013).

7. The depth interval from which a 1.15-m core of scaly-clay, identified as the fault zone in (*6*), extends from 7709.5 to 7714.3 mbsl in the coring hole 30 m away. In the logging hole, the fault is interpreted at 7709.5 to 7711.5 mbsl, 15 to 17 m above a decrease in rate of penetration associated with entering a hard chert layer at 7726.5 mbsl. A similar decrease in rate of penetration in the observatory hole is observed at 7727.5 mbsl. All depth correlations between holes contain an estimated several meters of uncertainty due to fluctuations of the ship's absolute elevation, flexure of the 7 km of drill stand, borehole deviation, layer-thickness variations, and fault dip.

8. E. Bullard, The time necessary for a bore hole to attain temperature equilibrium. *Geophys. J. Int.* **5**, 127–130 (1947). doi:10.1111/j.1365-246X.1947.tb00348.x

9. P. M. Fulton, R. N. Harris, D. M. Saffer, E. E. Brodsky, Does hydrologic circulation mask frictional heat on faults after large earthquakes? *J. Geophys. Res.* **115**, B09402 (2010). doi:10.1029/2009JB007103

10. T. Fujiwara, S. Kodaira, T. No, Y. Kaiho, N. Takahashi, Y. Kaneda, The 2011 Tohoku-Oki earthquake: Displacement reaching the trench axis. *Science* **334**, 1240–1240 (2011). Medline doi:10.1126/science.1211554

11. T. Lay, H. Kanamori, Insights from the great 2011 Japan earthquake. *Phys. Today* **64**, 33–39 (2011). doi:10.1063/PT.3.1361

12. S. Ide, A. Baltay, G. C. Beroza, Shallow dynamic overshoot and energetic deep rupture in the 2011 Mw 9.0 Tohoku-Oki earthquake. *Science* **332**, 1426–1429 (2011). Medline doi:10.1126/science.1207020

13. F. M. Chester, J. J. Mori, S. Toczko, N. Eguchi, the Expedition 343/343T Scientists, Japan Trench Fast Drilling Project (JFAST). *IODP Proceedings* 343/343T (2013).

14. C.-Y. Wang, M. Manga, *Earthquakes and Water*, vol. 114, Lecture Notes in Earth Sciences (Springer, Berlin, 2010).

15. J. E. Elkhoury, E. E. Brodsky, D. C. Agnew, Seismic waves increase permeability. *Nature* **441**, 1135–1138 (2006). Medline doi:10.1038/nature04798

16. K. Wang, T. Mulder, G. C. Rogers, R. D. Hyndman, Case for very low coupling stress on the Cascadia Subduction Fault. *J. Geophys. Res.* **100**, 12907–12918 (1995). doi:10.1029/95JB00516

17. G. Kimura, S. Hina, Y. Hamada, J. Kameda, T. Tsuji, M. Kinoshita, A. Yamaguchi, Runaway slip to the trench due to rupture of highly pressurized megathrust beneath the middle trench slope: The tsunamigenesis of the 2011 Tohoku earthquake off the east coast of northern Japan. *Earth Planet. Sci. Lett.* **339-340**, 32–45 (2012). doi:10.1016/j.epsl.2012.04.002

18. K. Ujiie, K. Ujiie, H. Tanaka, T. Saito, A. Tsutsumi, J. J. Mori, J. Kameda, E. E. Brodsky, F. M. Chester, N. Eguchi, S. Toczko, Expedition 343 and 343T Scientists, Low coseismic shear stress on the Tohoku-Oki megathrust determined from laboratory experiments. *Science* **342**, 1211 (2013).

19. K. Wang, K. Suyehiro, How does plate coupling affect crustal stresses in northeast and southwest Japan? *Geophys. Res. Lett.* **26**, 2307–2310 (1999). doi:10.1029/1999GL900528

20. W. Lin, M. Conin, J. C. Moore, F. M. Chester, Y. Nakamura, J. J. Mori, L. Anderson, E. E. Brodsky, N. Eguchi, B. Cook, T. Jeppson, M. Wolfson-Schwehr, Y. Sanada, S. Saito, Y. Kido, T. Hirose, J. H. Behrmann, M. Ikari, K. Ujiie, C. Rowe, J. Kirkpatrick, S. Bose, C. Regalla, F. Remitti, V. Toy, P. Fulton, T. Mishima, T. Yang, T. Sun, T. Ishikawa, J. Sample, K. Takai, J. Kameda, S. Toczko, L. Maeda, S. Kodaira, R. Hino, D. Saffer; Expedition 343 Scientists, Stress state in the largest displacement area of the 2011 Tohoku-Oki earthquake. *Science* **339**, 687–690 (2013). Medline doi:10.1126/science.1229379

21. G. R. Beardsmore, J. P. Cull, *Crustal Heat Flow* (Cambridge Univ. Press, Cambridge, 2001).

22. H. S. Carslaw, J. C. Jaeger, *Conduction of Heat in Solids* (Clarendon, Oxford, ed. 2, 1959).

23. R. H. Sibson, Thickness of the seismic slip zone. *Bull. Seismol. Soc. Am.* **93**, 1169–1178 (2003). doi:10.1785/0120020061

24. P. M. Fulton, R. N. Harris, Thermal considerations in inferring frictional heating from vitrinite reflectance and implications for shallow coseismic slip within the Nankai Subduction Zone. *Earth Planet. Sci. Lett.* **335-336**, 206–215 (2012). doi:10.1016/j.epsl.2012.04.012

25. A. Lachenbruch, U.S. Geological Survey, Simple models for the estimation and measurement of frictional heating by an earthquake (1986).

26. M. Kastner, H. Elderfield, W. J. Jenkins, J. M. Gieskes, T. Gamo, *Proc. Ocean Drill. Program Sci. Results* **131**, 397–413 (1993).